Optical Modeling Activities for NASA's James Webb Space Telescope (JWST): V. Operational Alignment Updates

Joseph M. Howard, Kong Q. Ha, Ron Shiri,
J. Scott Smith, Gary Mosier, Danniella Muheim

NASA Goddard Space Flight Center, Greenbelt, MD

ABSTRACT

This paper is part five of a series on the ongoing optical modeling activities for the James Webb Space Telescope (JWST). The first two papers discussed modeling JWST on-orbit performance using wavefront sensitivities to predict line of sight motion induced blur, and stability during thermal transients. The third paper investigates the aberrations resulting from alignment and figure compensation of the controllable degrees of freedom (primary and secondary mirrors), which may be encountered during ground alignment and on-orbit commissioning of the observatory, and the fourth introduced the software toolkits used to perform much of the optical analysis for JWST. The work here models observatory operations by simulating line-of-sight image motion and alignment drifts over a two-week period. Alignment updates are then simulated using wavefront sensing and control processes to calculate and perform the corrections. A single model environment in Matlab is used for evaluating the predicted performance of the observatory during these operations.

Keywords: Optical Modeling, Integrated Modeling, Telescopes, Phase Retrieval, Jitter, Thermal Stability

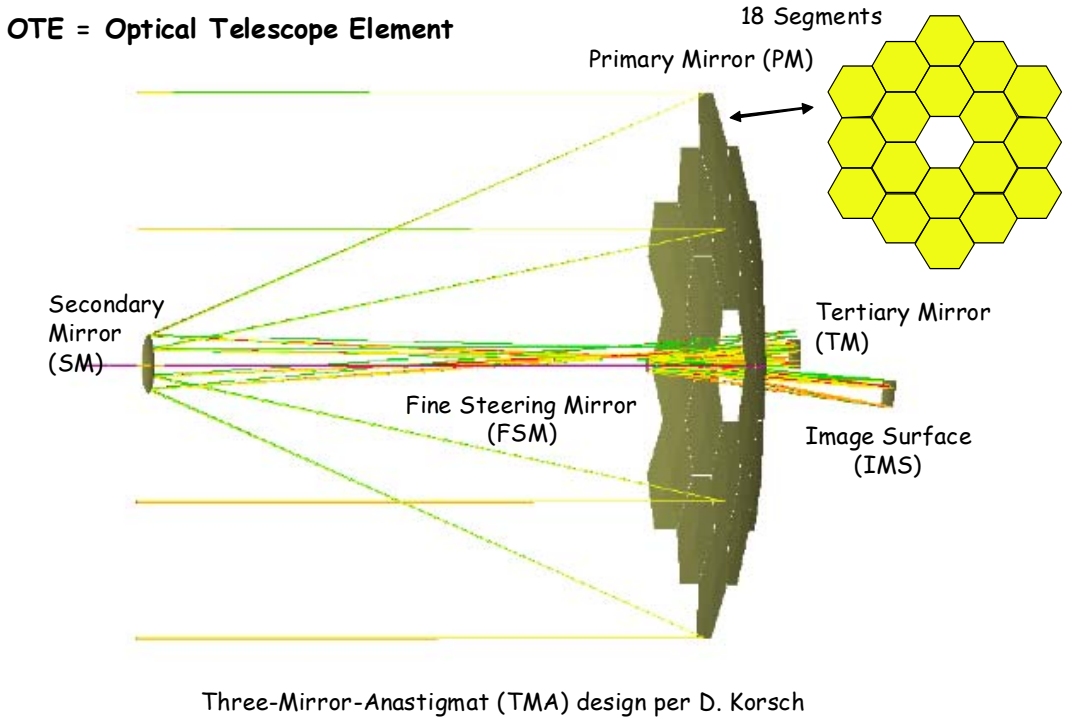

Figure 1. Optical Design of NASA's James Webb Space Telescope (JWST).

1. INTRODUCTION

The James Webb Space Telescope (JWST) is a large, infrared-optimized space telescope, scheduled for launch in 2013. JWST will find the first galaxies that formed in the early Universe, connecting the Big Bang to our own Milky Way Galaxy. JWST will peer through dusty clouds to see stars forming planetary systems, connecting the Milky Way to our own Solar System. JWST's instruments will be designed to work primarily in the infrared range of the electromagnetic spectrum, with some capability in the visible range [1].

The optical design of the telescope is a three-mirror-anastigmat (TMA), and is illustrated in Figure 1. Four optical surfaces are of interest: the segmented primary mirror (PM), secondary mirror (SM), tertiary mirror (TM), and the fast steering mirror (FSM). These optical surfaces belong to the "Optical Telescope Element", or OTE. The primary mirror is composed of 18 hexagonal segments, each of which span approximately 1.3 meters from flat to flat, giving the observatory a full aperture of over 6.5 meters. Both the primary and secondary mirrors are deployed after launch, requiring on-orbit alignment of the observatory, and phasing the primary mirror, which will be accomplished using image based wavefront sensing and control using the Near Infra-Red Camera (NIRCAM).

This paper is a collection of essays describing the efforts of the System's Verification and Analysis team (SVA) based at NASA's Goddard Space Flight Center. The NASA SVA team serves as an independent "cross-check" to the primary analysis performed by the contractor, lead by Northrop Grumman Corporation. NASA's SVA team uses separate modeling tools and independent analysis approaches, when reasonable. For example, while the NASTRAN structural models that are used are essentially common between the teams, the thermal models and optical models are different, and the methods to applying a thermal distortion analysis to the final optical performance outcome are distinct. As stated, this paper describes the cross-check modeling and analysis for JWST by NASA's SVA team, and does not attempt to report on the performance status as a whole for the observatory.

Assumptions and methods for modeling the operational cycle of JWST are discussed in Section 2, and a brief walk-through of the telescope (OTE) model, which includes detector models, are presented in Section 3. The wavefront sensing and wavefront control models are covered in Section 4, and some concluding remarks are offered in Section 5.

2. MODELING THE JWST SYSTEM

The JWST Optical performance requirements specify Strehl ratio (SR) and the stability of the encircled energy (EE) of the system point spread function (PSF) as image quality metrics. These metrics provide the measures of the sharpness and motion stability of images produced by the observatory. It is well known that SR is a direct function of the total wavefront error, whereas EE is dominantly affected by mid and high spatial frequency aberration and its stability is dictated by the time-variation of these spatial frequency components.

Mappings from the wavefront error to these metrics are well understood. Thus, models of the contribution of various optical components to the image quality can be given in terms of level of aberration and spatial frequency content of wavefront error. The JWST Optical performance budget is in this form, where RMS WFE is the metric which is distributed amongst the terms. A representation of the current budget is illustrated in Figure 2. To be more precise in the flow-down requirements, and to have closer prediction of performance based on characterization of wavefront error, aberrations are further categorized in terms of their spatial frequency regions. For JWST, this frequency decomposition is specified in terms of Zernike polynomial functions. The low spatial frequency region is represented by the first 22 fringe Zernike functions defined over the full JWST aperture. Aberrations whose frequency contents are in this region have less effect on the EE and its stability. The mid spatial frequency region is essentially defined to contain wavefront variations at the level equivalent to segment-to-segment variation. Most of the effects on the EE stability requirement will be caused by aberrations in this mid frequency region. High frequency region is in principle defined to contain wavefront error having essentially no component in the low and mid frequency regions. For JWST, it is simply constructed by a set of quilt patterns produced by the print-through of the back plane iso-grid structure, polishing patterns, and micro-roughness of the mirror surface. These patterns are likely to be static. To that extent, their contribution to the image quality is more in defining lower bound on the performance, i.e. upper bounds values on SR and EE, but not in any significant way on the EE stability.

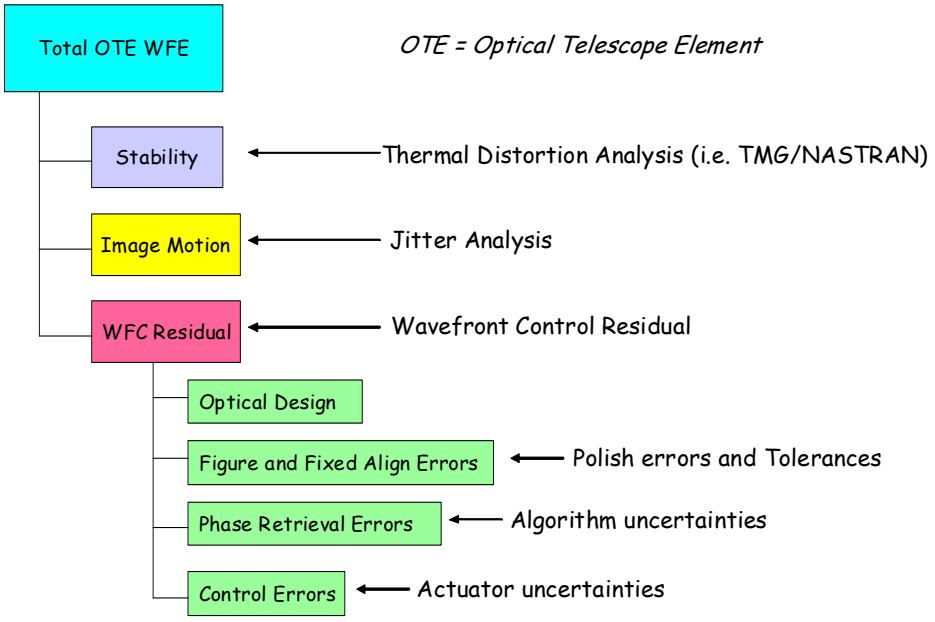

Figure 2. Optical Performance Budget of NASA's JWST.

There is another categorization of wavefront error used in establishing connection from time-varying physical responses of various structural components in the system to the image quality. There are essentially two types of time response effecting optical performance. There are perturbations from few tenths of Hz to hundreds of Hz due to high temporal frequency jitter, and there are low-frequency perturbations with time constants in hours to days, due to thermal distortions induced by thermal transient and settling after slewing. Perturbations associated with fast time responses are referred to as figure and alignment vibrate and those with slow time responses as figure and alignment drift. Here, alignment is associated relative change between primary mirror global structure (PM), secondary mirror (SM), aft optics including the tertiary mirror (TM) and fine steering mirror (FSM), and subsequent optical components in the optical path, e.g. science instruments. In a way, alignment refers to time-varying of low spatial frequency components. On the other hand, figure is referred to time-varying changes involving high spatial frequency contents equivalent to variation in primary mirror's segment level.

For JWST there are many significant optical wavefront error sources. In addition to static aberration due to design residual and figure error caused by optical polishing and fabrication, alignment error and almost every motion of any component in the system will induce some level of wavefront error that needs to be accounted for. This is due to JWST stringent performance requirements that are specified in nanometers for wavefront error and pointing uncertainty. To provide compensation, an active control system is designed to correct for low spatial frequency wavefront error utilizing phase retrieval to estimate the wavefront, and a linear estimation to derive optimal corrections in terms of controlled rigid body motions of the 18 segments and SM.

Since component drift and vibrate, as described above, are time-varying in nature, their effects on image quality in some cases can not be captured appropriately as wavefront error. Although they can be modeled as wavefront error given at an instant in time, it is the total effect of the motion over an extended period of time corresponding to a detector integration period is of interest. In that sense, drift and vibrate in optical components must be accounted for through the use of appropriate functions specified in PSF-domain to capture the direct impact they have on shape and spreading of the system PSF. For JWST, these PSF distortions are various noise sources in the detector signal processing and short-time responses to jitter at the optical components due to high frequency structural disturbances, and typically modeled as Gaussian blurs.

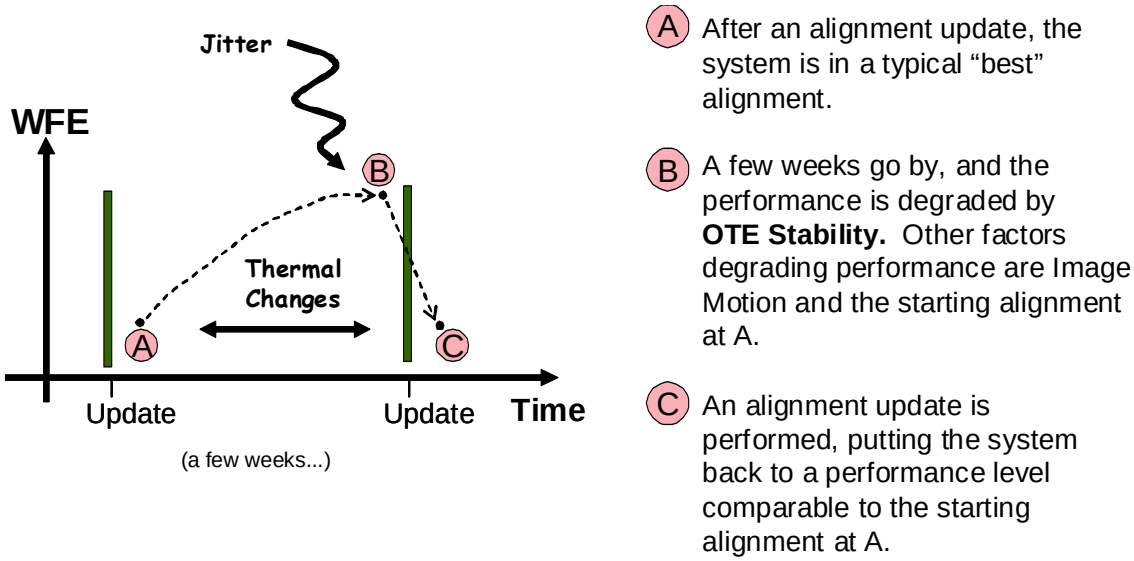

Figure 3. JWST Operational Alignment Update Cycle

Analyses supporting various independent verifications of JWST optical performance generally start by combining contributions in wavefront error and those in PSF-domain to construct system PSF functions that represent states of the optical system at various time periods. Image quality metrics are then computed from these PSF functions and check against requirements. A typical timeline and when PSF functions are to be computed is shown in Figure 3.

In the diagram, point **A** is shown to be the time right after a wavefront sensing and control is performed. An OPD map representing wavefront error containing uncorrectable components is generated to represent the system state at this point. This wavefront error map contain mostly component of spatial frequency outside of the control frequency, and is called the observatory wavefront control residual. It can also contain the reference OPD map used as commanded wavefront input to the wavefront control. Point B in the diagram represents the time right before a wavefront sensing and control, when the system has accumulated, in addition to the wavefront error at point A, all the time-varying aberration and drift in the system. Between point **B** and **C**, the wavefront error is reduced by an application of a wavefront sensing and control. At point **C**, RMS of the corrected wavefront error should be comparable to that at point **A**. This is actually dependent on not only the amount of mid and high spatial frequency component in the drift terms during period between point **A** and point **B**, but also how active the vibrate terms happen to occur at point **B**. In addition, different command wavefront can play an important role in the variation of the wavefront error at point **C**.

Constructing OPD maps with different frequency contents and amplitude is clearly an important step in the verification of performance by analysis. To do this, a process that is capable of constructing OPD maps based on specified Zernike composition at both full aperture and segment level has been developed. This process also performs DFT and is capable of incorporating effect on PSF through OTF. This process has been extended to handle and include various predicted results from other analyses in the verification effort. This process is developed to support the verification of the optical error budget and the WFSC.

Although the spatial frequency regions defined in the error budget as low and mid are not explicitly required to be orthogonal, in the forming of OPD map based on Zernike composition for low and mid frequency wavefront errors, the process removes the correlation between the wavefront maps of the low and mid frequency, so that the two wavefront maps are essentially orthogonal. This is to ensure that root sum squared of all the spatial frequency components will yield the same total RMS given in the error budget.

To verify the optical error budget with this process and based on the time line suggested in Figure 3, we perform the following steps which are graphically illustrated in Figure 4:

- Based on the Zernike composition specified in the error budget for the observatory wavefront control residual, an initial wavefront map is generated for point A.
- Another wavefront error map is generated for OTE stability that includes various low order Zernikes with significant amplitude and RMS values.
- By combining to get total wavefront error at point B, the transformation to PSF is then performed. Gaussian blur with specified direction for x, y variances based on jitter level given in error budget can be convoluted with the PSF to result in the detected PSF.
- Various detector noises are then added to the PSF, and depending on the object magnitude, the signal-to-noise ratio can be computed. The result is a read-out PSF that is first defocused by specified number of waves and then used as input to the wavefront sensing phase retrieval process.
- The phase retrieval process produces recovered OPD map from the input read-out PSF, which is used as input to the wavefront control process, along with a reference commanded wavefront.
- The wavefront control process essentially performs an inverse mapping based on an optimal estimation approach to generate commanded actuator corrections that nominally minimize the error between the recovered OPD map and commanded wavefront map.
- Based on actuator quantization values, these actuator corrections are mapped to their actual values, and are applied to the actuators.
- An actual wavefront error is then constructed either based on ray-trace or linear sensitivity.
- Image quality calculation is performed using all wavefront error maps produced in the above steps and the results are checked against the requirements.

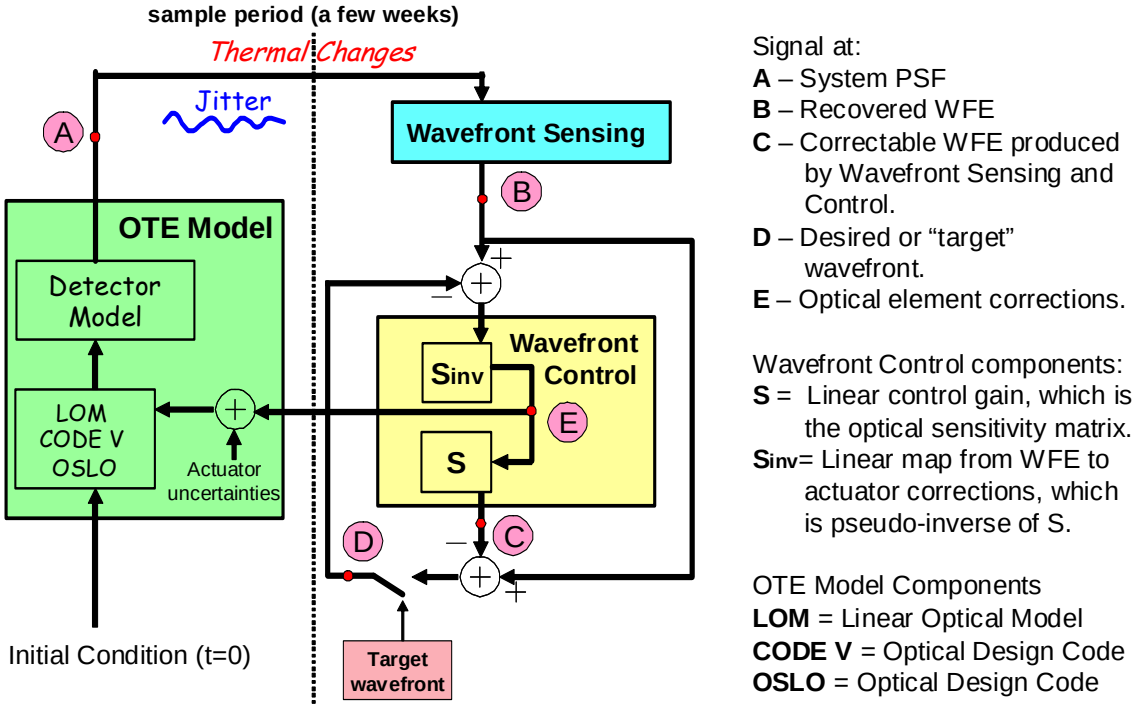

Figure 4. System control model for JWST Alignment updates

Typically, the above steps are performed in a Monte-Carlo simulation run. With many parameters that can be randomized, studies so far have been confined mainly on the impact of relative bright objects for WFSC, various levels and shapes of Gaussian blur, and different initial control residuals.

WFE due to OTE stability generated either from SDR4+ or allocated values leads to IQ well within requirement (between Point A and B). Effects due to jitter at the level specified in EB on WFS/PR and IQ are not significant.

Based on current radiometric models, radiometric noise input to WFS/PR from 8.5 visual magnitude or brighter sources has little or no effect on PR performance. Effects due to actuator quantization specified in EB is not significant. Still, need to determine effect due to uncertainty in WFC input reference OPD, and better wavefront control scheme to not only minimize WFE and corrections, but also be adaptive to get better solutions.

3. OTE MODEL

The JWST OTE is modeled optically in three ways: using a linear optical model (LOM), using raytrace data from CODE V [2], and using ray trace data from OSLO [3]. The LOM is discussed at length in Reference [4], and interfacing Matlab with CODE V and OSLO is discussed at length in Reference [5]. For the bulk of the analysis to date, the LOM has been the workhorse for serving as the OTE model [6-7]. Essentially it is a collection of optical wavefront sensitivities (or derivatives) taken from the optical model, where each surface of interest is moved in rigid body. Figure 5 illustrates the sensitivities for the PM, SM, and TM. Note that each optic is symmetric about the Z axis, thus the sensitivity for rotation about Z is essentially zero.

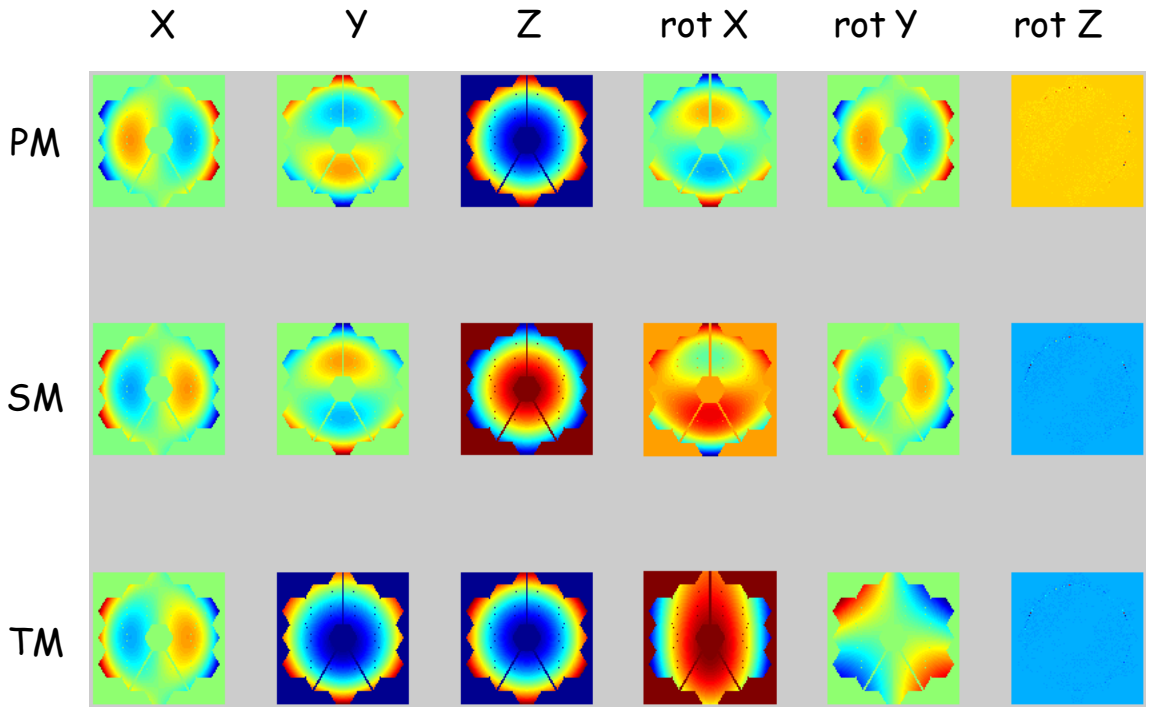

Figure 5. Linear Optical Model JWST simulations.

This "stack" of matrices can then simulate any system perturbation (in rigid body) by simple multiplication by the value of the perturbation. Analysis has shown that the accuracy of this model is within a percent out to the mm and mrad level of perturbation. As with the rest of the models discussed here, the LOM is Matlab-based.

The detector is modeled as a series of operations on the wavefront maps produced by either the LOM or the optical raytrace model. The essential steps to model the noise associated with detector processes are listed as follows:

Compute PSF at the detector

1- Start with PSF computed for given WFE and aperture geometry for wavelength L in specified wavelength set.
2- Multiply this PSF point-by-point with Spectral Energy Density (SED) data at wavelength L
3- Add stray light, Zodi, and Thermal emission (all with noise) to each pixel
4- Add Jitter effects
5- Accumulate the result derived here over all wavelengths to build the PSF at the detector.

Compute detected PSF
6- Bin the PSF into detector pixel size.
7- Multiply this binned PSF with QE data of wavelength L (with noise)
8- Accumulate the result here over all wavelengths to build the detected PSF.

Compute readout PSF
9- Add dark current (with noise), and read noise
10- Quantize this corrupted binned PSF at each pixel with given quantization level to build the readout PSF.

Compute processed PSF
11- From the readout PSF, compute the mean over a user selected region in the PSF space to obtain noise floor.
12- Subtracted from each of the pixels in the readout PSF this computed noise floor to build the processed PSF.

This process is contained in a graphical user interface (GUI), and is illustrated in Figure 6.

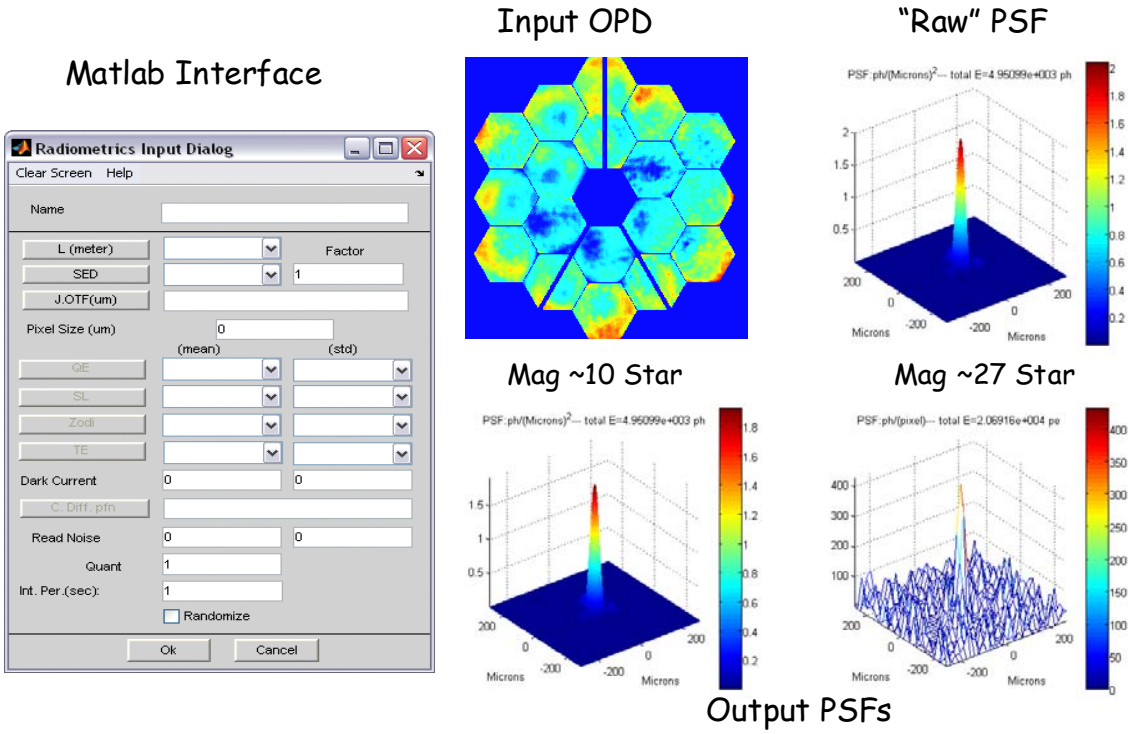

Figure 6. Detector Model Interface and outputs.

4. WAVEFRONT SENSING AND WAVEFRONT CONTROL MODELS

As part of the JWST government team, we have developed and present an independent realization of the wavefront sensing software and algorithms of the previously technology reported by Ball Aerospace and GSFC [8]. The fine-phasing algorithm is the Hybrid Diversity Algorithm (HDA), which incorporates the benefits of an iterative transform phase retrieval algorithm and a parametric phase retrieval algorithm.

The James Webb Space Telescope (JWST) requires an image-based wavefront sensing algorithm in four of the seven commissioning steps to align the telescope upon deployment in space. Furthermore, the final two steps of the commissioning process will be repeated periodically (currently planned for every 14 days) to ensure the continued optimal performance of the telescope. The image-based wavefront sensing algorithm selected for JWST to be used in conjuncture with the Near Infrared Camera (NIRCam) is the Hybrid Diversity Algorithm (HDA). Far in advance of launch, the JWST project requires an implementation of the HDA for many aspects of developing the telescope,

including integrated modeling and tolerancing and ground verification and testing of sub-components and the entire system. Thus, the software described in the present document has been developed to meet these wide-ranging needs.

The software is capable of determining optical wavefront information, using as input a variable number of irradiance measurements collected in defocused planes about the best focal position. The software also uses input of the geometrical definition of the telescope exit pupil (otherwise referred to as the “pupil mask” or just the "mask") to identify the JWST 18 primary mirror segment locations. Using the irradiance data and mask information, the software calculates an estimate of the optical wavefront of the telescope generally and across each primary mirror segment specifically. The software is capable of generating irradiance data, wavefront estimates, and basis functions for the full telescope and for each primary mirror segment, or optionally, each of these pieces of information can be measured or computed outside of the software and incorporated in its operation.

As focused in this paper, the wavefront sensing software is used as part of the integrated modeling effort at NASA / GSFC, to provide an end-to-end model of the telescope. Using STOP analysis, realizations of the telescope are generated that are representations that met the system requirements. The output from this analysis is a wavefront, and one realization can be seen in Figure 6. From this, we used a Fourier Propagation to construct a near ideal PSF that accounts for a polychromatic source, global and figure vibrate, potential ghosts and scattering, Zodi background noise, and minimizing the effect aliasing in the PSF due to sampling and the FFT. This PSF is then passed through our detector model that accounts for all of the known detector noise effects. In Figure 7, we show the PSF including these various effects for the ±8 waves of diversity defocus weak lenses, as well as the in-focus PSF. In addition to the PSFs, the HDA software requires the pupil amplitude and knowledge of the weak lenses. To account for uncertainty in the pupil amplitude and weak lenses, we used modified, but different, versions of these quantities for constructing the PSF and for the input the HDA software. This includes apodization, geometric distortion uncertainty, and weak lens wavefront uncertainty.

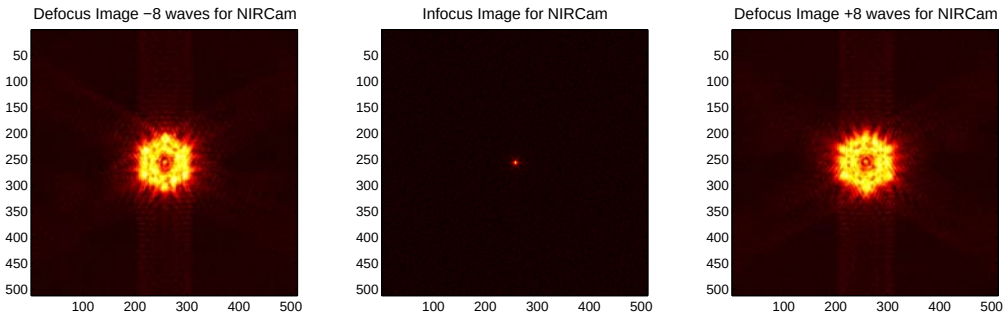

Figure 7. PSF input for wavefront sensing model

Given all of these modeled noise sources and uncertainties, the HDA software was able to recover the original wavefront for all realization to 10 nm RMS over the low-order aberrations, Zernike 2-15, and 10 nm RMS of the mid frequency content, 6 degree of freedom motion and power for primary mirror segments. The recovery, in frequency space, beyond the low and mid terms becomes of interest for verification of the telescope, but is outside the controllable modes.

Wavefront Control

The wavefront control and optimization process for JWST involves control of 18 primary segmented mirrors in addition to the secondary mirror. The total degrees-of-freedom (DOF) per mirror includes the rigid body motion of three positions and three orientations. Further, each segment has additional radius of curvature (ROC). In total, there are 132 degrees of freedom to adjust and align the telescope for a desired orientation and direction.

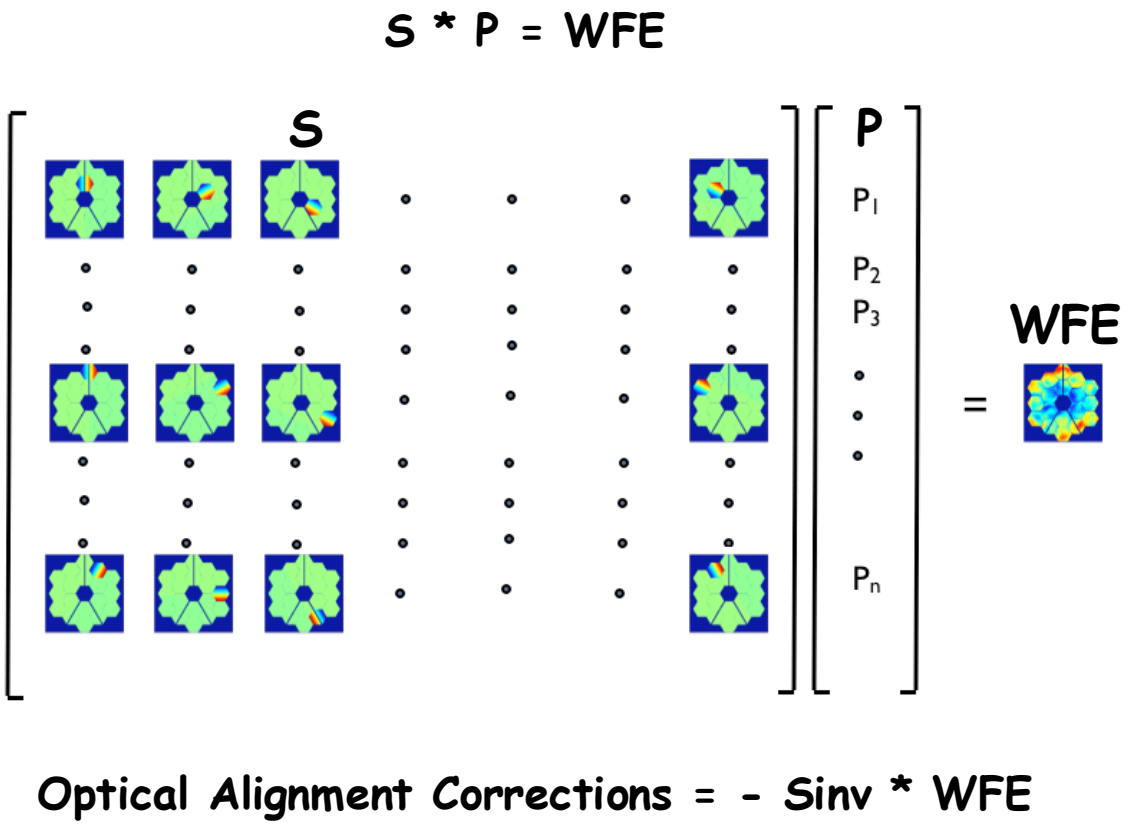

Figure 8. Wavefront Control Model.

The control of JWST in fine phasing process is inherently linear but because of large number of DOFs the task of finding an optimal alignment for a particular direction is non-trivial. Similarly, the global alignment of the telescope requires coordination of secondary mirror DOFs for an optimal direction. Mathematically, the wavefront control of JWST can be summarized into a linear matrix solver in the form of $\mathrm{A}x = b$ where A is an influence matrix, b is vector of target wavefront map and x is the desired perturbation to be applied to each segment. Figure 8 shows the content of the influence matrix, the perturbation vector and target wavefront map. In this context, an influence matrix is constructed by perturbing each controllable mode, the rigid-body modes associated with each mirror, within the linear range and record the optical path difference (OPD) wavemap from the optical model. The difference between the perturbed wavemap and nominal wavemap provides the basis of the influence function [9].

Given the over-determined influence matrix (more rows than columns) and high condition number, is equivalent to saying the matrix is in certain sense close to singular and as result the general least square solution produce results with poor numerical stability. Alternatively, Singular Value Decomposition (SVD) can be employed as a least square method to obtain the optimal solution in terms of the controllable and observable modes and eliminate the modes which are associated the numerical instability. This method is based on matrix factorization of rectangular matrix A into three matrices in the form of $\mathrm{A} = \mathrm{USV}^{\mathrm{T}}$ where U and V are orthogonal matrices and S is a diagonal matrix that contains the singular values [10]. The diagonal vector in the S matrix is ordered such that their singular values are decreasing $s_1 \geq s_2 \geq \mathrm{L} \geq s_n \geq 0$ where s_i is the ith singular value. Taking the inverse of S with non-zero singular values and setting the smallest and zero singular values to zero, an inverse of A is constructed and ultimately x vector could be obtained from $x = \mathrm{VS}^{-1}\mathrm{U}^{\mathrm{T}} b$. The SVD matrix formalism in the least square sense, determines by how much to perturb each degree of freedom in order to bring the optical system from its current state to the target state as best as possible.

5. CONCLUDING REMARKS

To date, no significant issues have been found with JWST meeting the requirements for operations and alignment updates. The system level modeling discussed here will soon be applied to the verification program for the observatory, where tests will be modeled to ensure the uncertainties are within specification. Additionally, these tools will be used to perform "blind testing" of the contractor teams to simulate the initial commissioning of the observatory.

REFERENCES

[1] Please visit http://www.jwst.nasa.gov for the latest overview of NASA's James Webb Space Telescope.
[2] CODE V is a trademark of Optical Research Associates, Pasadena, CA.
[3] OSLO is a trademark of Lambda Research Corporation, Littleton, MA.
[4] Joseph M. Howard, "Optical modeling activities for the James Webb Space Telescope (JWST) project: I. The linear optical model," Proc. SPIE 5178, 82 (2004).
[5] Joseph M. Howard, "Optical modeling activities for the James Webb Space Telescope (JWST) project: IV. Overview and Introduction of Matlab based toolkits used to interface with optical design software" Proc. SPIE 6668 (2007).
[6] Joseph M. Howard and Kong Ha, "Optical modeling activities for the James Webb Space Telescope (JWST) project: II. Determining image motion and wavefront error over an extended field of view with a segmented optical system," Proc. SPIE 5487, 850 (2004).
[7] Joseph M. Howard, "Optical modeling activities for the James Webb Space Telescope (JWST) project: IV. Wavefront Aberrations due to Alignment and Figure Compensation," Proc. SPIE 6675 (2007).
[8] Bruce Dean, D. Aronstein, J. S. Smith, R. Shiri, D. S. Acton. "Phase retrieval algorithm for JWST Flight and Testbed Telescope", Proceedings of SPIE (2006) vol. 6265 (11).
[9] R. Shiri, D.L. Aronstein, J.S. Smith, B. Dean, and E. Sabatke, 'Wavefront Control Toolbox for James Webb Space Telescope', Proc. SPIE 6711, 67110P, 2007.
[10] H. N. Chapman and D. W. Sweeney, 'A Rigorous Method for Compensating Selection and Alignment of Microlithographic Optical Systems', Proc. SPIE, 3331, 1998.